Gas-Phase Collision Induced Dissociation Mechanisms of Peptides: Theoretical and Experimental study of N-Formylalanylamide Fragmentation

Daniel Ortiz, Pablo Martin-Gago, Antoni Riera, Kihyung Song, Jean-Yves Salpin, Riccardo Spezia

Gas-Phase Collision Induced Dissociation Mechanisms of Peptides. Theoretical and Experimental Study of *N*-Formylalanylamide Fragmentation.

*Daniel Ortiz[1,2], Pablo Martin-Gago[3], Antoni Riera[3], Kihyung Song [4], Jean-Yves Salpin[*1,2] and Riccardo Spezia[*1,2]*

1) Université d'Evry Val d'Essonne - Laboratoire Analyse et Modélisation pour la biologie et l'Environnement, Boulevard François Mitterrand, 91025 Evry Cedex (France).

2) CNRS- UMR 8587.

3) Institute for research in Biomedicine (IRB Barcelona) and Departament de Química Orgànica, Universitat de Barcelona. Baldiri Reixac, 10, E-08028 Barcelona (Spain).

4) Department of Chemistry, Korea National University of Education, Chungbuk (Korea)

Correspondence to:riccardo.spezia@univ-evry.fr; jean-yves.salpin@univ-evry.fr

ABSTRACT

In order to shed light on the fragmentation mechanisms occurring during the collision induced dissociation (CID) of peptides in the gas phase, we have studied a peptidic model system, the *N*-Formylalanylamide (HCO-Ala-NH_2), by coupling experimental and theoretical methods. In particular, we have addressed two different questions arising in such experiments: i) what is (are) the structure(s) of the ion before collision, and ii) what are the fragmentation mechanisms occurring after collision with the target gas. For the first question, we coupled the potential energy surface (PES) study done by means of density functional theory (DFT), with InfraRed Multiple Photon Dissociation (IRMPD) spectroscopy. For the second problem, which is actually the main topic of the present work, we coupled quantum mechanics plus molecular mechanics (QM+MM) direct chemical dynamics simulations with tandem mass spectrometry (MS/MS). In addition, in order to better delineate the fragmentation mechanisms and validate those proposed by simulations, isotopic labeling experiments using ^{2}H and ^{13}C were performed. Thanks to the interplay between simulations and experiments, it was possible to successfully identify the fragmentation pathways leading to b_1, y_1, a_1 and immonium ions. Our mechanisms support the "mobile proton" picture that is supposed to trigger the peptide fragmentation in the gas phase, confirming, from a chemical dynamics point of view, previous theoretical and experimental studies on similar systems.

Keywords: Collision Induced Dissociation; Peptide gas phase fragmentation; Molecular dynamics; Infra Red Multiple Photon Dissociation; QM+MM chemical dynamics

1. INTRODUCTION

Protein identification in proteomics is primarily based on sequencing of proteolytic peptides by means of tandem mass spectrometry (MS/MS).[1-3] In these experiments, ions are usually sampled from a atmospheric-pressure electrospray source into the first mass analyzer that is operated in the mass filter mode to selectively transmit the desired precursor ions. The selected ions are accelerated into the collision cell where excitation and dissociation take place by collision-induced dissociation (CID). The second mass analyzer is used to record the *m/z* values of the dissociation products.[4] In the limit of low-energy collisions, electronic excitation is unimportant and collisions transfer a fraction of the translational energy both to vibrational and rotational energy of the ion. Several research groups have used CID to decipher peptide sequences by means of bioinformatic tools.[5-7] These software products utilize fragmentation models to generate theoretical spectra for candidate sequences, measuring the similarity between theoretical and experimental spectra: the spectrum that best matches the experimental one is used to assign the sequence. Nevertheless, the uncertainty in the evaluation is one of the limiting factors in large-scale protein identification studies. This explains the importance of understanding the fragmentation processes of protonated peptides and, therefore, the necessity to developnew techniques in order to study CID process.

Different authors have studied fragmentation of protonated peptides obtaining different possible fragments (and fragmentation pathways). Backbone cleavage at amide bonds, leads to N-terminal, b_n^+, and C-terminal, y_n^+, ions, but also, after successive decomposition a_n^+ ions are obtained.[8-15] In terms of decomposition leading to the losses of small neutrals, the elimination of water has long been investigated.[16, 17] Loss of CO was found to be coupled to proton mobility in protonated diglycine [18, 19] and the same loss of CO was obtained from the intermediate oxazolone structure by Paisz *et al*.[20] Oxazolone structure (a cyclic type b ion) formation was described in detail by Paisz *et al*. through accurate quantum chemical calculations for $HCO\text{-}CH_2\text{-}CO\text{-}NH_2$ and MeCO-CHMe-CO-

NH_2.[21] Note that the formation of such oxazolone structure was first proposed by Harrison and co-workers [22] and later the first evidence was provided by IRMPD experiments by Polfer *et al*.[23] Finally, the loss of N-terminal acyl (formyl) group was reported by Komaromi *et al*.[24] in a model study of N-acetyl O-methoxy proline where it was pointed out a competition between low energy process, leading to methanol loss and high energy process, leading to ketene loss. The lacking of ammonia elimination from the N-terminal side was explained as due to the lack of stable fragments and presence of competitive exit channels.[25, 26]

A crucial step in the peptide fragmentation mechanisms is attributed to the proton mobility induced by energy activation after collision. The mobile proton model, which describes how protonated peptides dissociate under low-energy collisions, has been described by several groups by both theoretical and experimental methods.[27-32] In protonated peptidic systems, the added proton moves through protonation sites allowing charge-directed fragmentations. Paizs, Suhai and coworkers described a theoretical model [28] in which the proton transfer processes connect different protonation sites of protonated diglycine. Both, RRKM and DFT calculations were used to conclude that the proton transfers between conformers were found to be fast with relatively low energy barriers. Furthermore, when CID occurs the internal energy of the ion increases upon excitation. Consequently, energetically less favored protonation sites become more populated. This means that for systems like peptides, where different protonation sites are available, they become, after activation, energetically accessible.

The molecular picture of these mechanisms being clarified by studies of potential energy surface (PES) and statistical unimolecular reactions (i.e. RRKM methods), we are interested in show how (and if) chemical dynamics simulations can reproduce these mechanisms and improve our knowledge on them. Chemical dynamics in the gas phase, in fact, can be seen as a complementary picture of PES and RRKM studies, in providing non-statistical or non-kinetics effects or more in general the “short” time-scale behavior of chemical reactions. Example can be found in the case of $[Ca(urea)]^{2+}$ CID fragmentation

mechanisms,[33] shattering mechanism in surface induced dissociation (SID) of protonated octaglycine,[34] CID and SID of protonated glycine,[35] CID of CH_3SH^+, CH_3SCH^{3+}, $Cr^+(CO)_6$, H_2CO^+ and protonated urea.[36-42]

In the present work we have focused our attention on a synthesized model system, the N-Formylalanylamide, HCO-Ala-NH_2 (shown in Figure 1), that is a multifunctional peptide model bearing four protonation sites. Due to the relatively small size of such a model, it is possible to perform not only calculations at different theoretical levels, but also chemical dynamics. Furthermore, the relatively easy interpretation of CID and IRMPD experiments allows a full comparison between experiments and simulations.

The main purpose of the present study is to obtain a detailed picture of the reaction mechanisms involved in CID. Generally, CID experiments are interpreted by inspecting the PES that can give information on reactants, products and transition states, connecting them with satisfactory results for many systems.[43-45] Nevertheless, depending on the system, limitations must be taken into account when only the PES is considered: (i) the PES can give insights on statistical fragmentation but does not take into account any kinetic effect and (ii) all possible isomers and fragmentation pathways have to be considered. This becomes difficult for large systems not only for computational reasons but also because of conformational congestion. Direct dynamics can overcome these problems since the system (with the necessary statistical sampling) is allowed to experience pathways that are activated due to energy transfer subsequent to collision.

In the present work, we combine QM+MM direct dynamics simulations with the aforementioned experimental techniques (CID and IRMPD) on HCO-Ala-NH_2, which then leads to the protonated form $[(HCO\text{-}Ala\text{-}NH_2)H]^+$ under electrospray conditions. Furthermore, ^2H and ^{13}C labeling ESI-MS/MS experiments were carried out to gain some insights about the fragmentation pathways, in order to

confirm the results obtained from direct dynamics simulations. By coupling simulations to experiments, we were consequently able to propose consistent fragmentation mechanisms accounting for the various fragment ions observed experimentally.

2. MATERIALS AND METHODS

2.1.Chemicals

Syntheses of the products HCO-Ala-NH_2 and isotopic-labeled DCO-Ala-NH_2 and $H^{13}CO$-Ala-NH_2 were carried out as described in the Scheme 1 by using Rink Amide MBHA resin as solid support.

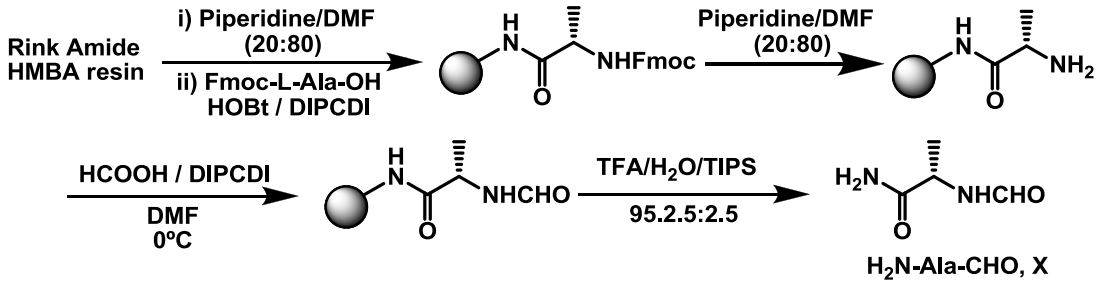

Scheme 1:*Synthesis of HCO-Ala-NH_2 (X). Labeled compounds DCO-Ala-NH_2 (Y) and $H^{13}CO$-Ala-NH_2 (Z)* were prepared by an analogous procedure.

The coupling of the Fmoc-L-Ala-OH was done in DMF in the presence of *N,N'*-diisopropylcarbodiimide (DIPCDI) and 1-hydroxybenzotriazole (HOBt). Piperidine 20% in DMF was used for Fmoc- removal. *N*-Formylation of the terminal amine was accomplished in DMF at low temperature, by using a mixture of DIPCDI and formic acid (HCOOH, DCOOH or $H^{13}COOH$, respectively). Finally, treatment of the resin with a cleavage cocktail (TFA/H_2O/TIPS) allowed us to obtain the desired product with moderated yields and excellent purities. The reaction conditions as well as the NMR data are summarized in the Supporting Information (SI-A).

2.2. Mass spectrometry Experiments

Experiments were performed using an Applied Biosystems/MDS Sciex API2000 triple-quadrupole instrument fitted with a turboionspray ion source. Aqueous solutions of HCO-Ala-NH_2 (10^{-4} M) were prepared in pure water (purified with a Milli-Q water purification system) and were introduced into the source using direct infusion with a syringe pump at a flow of 5 µl/min. Ionization of the sample was achieved by applying a voltage of 5.5 kV on the sprayer probe and by the use of a nebulizing gas (GAS1, air) surrounding the sprayer probe, intersected by a heated gas (GAS2, air) at an angle of 90°. The operating pressure of GAS1 and GAS2 are adjusted to 2.1 bars, by means of an electronic board (pressure sensors), as a fraction of the air inlet pressure. The curtain gas (N_2), which prevents air or solvent from entering the analyzer region, was similarly adjusted to a value of 1.4 bars. The temperature of GAS2 was set to 100°C. CID spectra were recorded by introducing N_2 gas in the second quadrupole at a total pressure of 3 x 10^{-5} mbar. Moreover, declustering potential was fixed at 20 V to perform MS/MS experiments. CID spectra were recorded at different collision energies ranging from 6 to 20 eV (laboratory frame).

2.3. IRMPD Experiments

The present IRMPD spectroscopic investigation has been performed using an experimental platform which has been described in details previously.[46] This platform coupled a modified quadrupole ion trap (Bruker, Esquire 3000+) mass spectrometer to the IR free electron laser (FEL) of the CLIO (Centre Laser Infrarouge d'Orsay) center.[47] The FEL system is based on a 16-48 MeV linear electron accelerator where bunches of electrons are injected in the alternating magnetic field placed in the optical cavity. Wavelength tunability of this laser system is achieved at fixed electron energy by changing the gap between magnets. For the experiments in the 1100-1900 cm^{-1} spectral region, the electron energy was fixed at 45 MeV and a stable average power of 800-1000 mW was observed.The IR FEL delivers 8 μs long trains of macropulses at a repetition rate of 25 Hz. Each macropulse conveys typical energies of

40 mJ. A conical hole (0.7 mm of diameter) in the ring electrode of the trap was made in order to allow the optical access to the centre of the trap.

Multistage mass spectrometry was carried out using the standard Bruker Esquire Control (v 5.2) software. In order to record the IRMPD spectrum, the $[(HCO\text{-}Ala\text{-}NH_2)H]^+$ cation was mass-selected in the MS^1 step and the control of the irradiation time (typically 200 ms) was obtained using the MS^2 step. Mass spectra were averaged over 15 accumulations using the standard mass range (m/z 50-3000) and the normal scan resolution (13000 Th s^{-1}). This sequence was repeated 10 times for each recorded frequency.

2.4 Computational details

Potential energy surface (PES). Geometry optimizations of minima and saddle points and fragmentation products of protonated HCO-Ala-NH_2 were obtained by combining the B3LYP functional [48, 49] with the 6-311++G(d,p) basis set. Harmonic vibrational frequencies were computed at this level, and zero-point vibrational energy (ZPE) were added to the relative energies refined with the extended 6-311++G(2df,2p) basis set. PM3 semiempirical Hamiltonian was also used, starting from B3LYP minima, to investigate the potential energy surface (PES) with the same level further used in the direct dynamics simulations. All these calculations were performed by means of Gaussian03 suite of programs.[50]

Here and hereafter we use the following nomenclature to identify each structure: the first two characters are in common for all structures (AH) and mean protonated (H) alanine (A); the third character is a number which refers to the protonation site, being 1 (amide nitrogen), 2 (amide carbonyl), 3 (secondary amide) and 4 (formyl group), as shown in Figure 2; the last character is a letter denoting different conformers for the same isomer (i.e. the same protonation site).

With the aim to describe more in detail the proton shuttling between both carbonyl groups (**AH2_a**, **AH4_a** and **TS1**), MP2/6-311++G(d,p) calculations were also performed.

Direct dynamicssimulations. The potential energy function for the collision system, consisting of protonated $[(HCO\text{-}Ala\text{-}NH_2)H]^+$ ($peptide^+$) and the collision gas (Ar) is described by:

$$V = V_{peptide^+} + V_{Ar-peptide} \qquad (1)$$

where $V_{peptide+}$ is the intramolecular potential of protonated HCO-Ala-NH_2 and $V_{Ar\text{-}peptide}$ is the Ar/$[(HCO\text{-}Ala\text{-}NH_2)H]^+$ intermolecular potential. The PM3 semiempirical Hamiltonian has been used for the intramolecular potential. B3LYP/6-31G* intramolecular potential was also used for one short time set of simulations in order to check the reliability of PM3-based dynamics. Note that B3LYP-based chemical dynamics simulations are much more computationallyexpensive and even if based on a more reliable potential, they will necessarily suffer from a lack of enough statistical sampling.

The intermolecular potential is expressed as a sum of two-body terms between the collision gas and the atoms of $[(HCO\text{-}Ala\text{-}NH_2)H]^+$, with each two body term given by :

$$V_{Ar-peptide} = \sum_i A_{Ar-i} e^{-B_{Ar-i} r_{Ar-i}} + \frac{C_{Ar-i}}{r_{Ar-i}^9} \qquad (2)$$

where *i* runs over all the $[(HCO\text{-}Ala\text{-}NH_2)H]^+$ atoms. This potential is purely repulsive – A, B and C are always positive – and it was developed by Meroueh and Hase to simulate CID of protonated peptides.[37] Values for A,B and C are listed in the supporting information (SI-B). The same potential of Eq. 2 was recently used to simulate CID of protonated urea and $[Ca(urea)]^{2+}$, and good agreements with experimental results were obtained.[33, 36, 37]

Note that here, as previously mentioned, we used Ar in simulations while in experiments N_2 is used as collision gas. As we have recently shown in a simple model case,[37] the main difference is that Ar gas

provides a more efficient energy transfer with respect to N_2 and higher reaction probability (55% vs 30% in case of protonated urea).

Chemical dynamics simulations were performed for the following isomers: **AH1, AH2_c, AH3, AH4_a, AH4_b**. They correspond to the minimum energy structure in the PES for each possible protonation site. We also added the **AH2_a** conformer since it lies only few kJ/mol higher in energy than **AH4_a**. Structures are shown in Figure 2.

Initial conditions for each isomer were chosen by adding a quasi-classical 300 K Boltzmann distribution of vibrational/rotational energies about the isomers potential energy minima.[51-53] Energies for the normal modes of vibration were selected from a 300 K Boltzmann distribution. The resulting normal mode energies were partitioned between kinetic and potential energies by choosing a random phase for each normal mode. A 300 K rotational energy of RT/2 was added to each principal axis of rotation for the ion. Vibrational and rotational energies were transformed into Cartesian coordinates and momenta following well-known algorithms implemented in VENUS.[54, 55] The ion was then randomly rotated about its Euler angles to take into account the random directions of the Ar + $[HCO\text{-}Ala\text{-}NH_2)H]^+$ collisions. Relative velocities were then added to the Ar/$[(HCO\text{-}Ala\text{-}NH_2)H]^+$ system in accord with the center-of-mass collision energy and impact parameter. Collision energy of 8.6 eV (836.8 kJ/mol) was considered, corresponding to laboratory frame energy of 11 eV (1060.0 kJ/mol). The impact parameter, b, was randomly sampled between 0 and 2.5 Å. The trajectories were calculated using a software package consisting of the general chemical dynamics computer program VENUS 96 coupled to MOPAC.[56] It was used to calculate the potential energy and gradient for the protonated peptide intramolecular potential. The classical equations of motion were integrated using the velocity Verlet algorithm with a time step of 0.2 fs that gives energy conservation for both reactive and nonreactive trajectories. The trajectories were initiated at an ion-projectile distance of 15 Å, large enough to guarantee no interaction between the ion and the colliding atom, and halted at a distance of

300 Å to allow substantial intramolecular motion of the protonated peptide ion. This corresponds to a total integration time of about 50 ps. A trajectory was also stopped if the ion dissociates. In that case, the criterion distance of 7 Å was also used to guarantee no interactions between fragments. For each isomer, approximately 5000 trajectories were performed.

The B3LYP/6-31G* chemical dynamics simulations were done using as initial structure the **AH4_a** isomer (the most stable form) and with same initial condition generation method as PM3-based dynamics. The VENUS 96 code [54, 55] coupled to Gaussian03 [50] was employed. In this case, due to the large computational time needed to run dynamics on such a relatively big system, only 125 trajectories were performed. Simulations were initiated at 5 Å and halted at 10 Å for a total simulation time of about 0.2 ps per trajectory. These results, while lacking enough statistical sampling, can give clues on reliability of PM3-based simulations.

Note that our chemical dynamics simulations model the "ideal" medium-energy single collisions, while in real experiments there are surely multiple collisions, even when the set-up tries to minimize their number (see section **XX**). Further, other experiments in the litterature directly implement multiple low-energy collisions to obtain fragmentation. Our simulations thus can be qualitatively comparable with experiments with fewest collisions while the comparison with multiple low-energy collision is more subtle: we are in the limit in which energy is given in a single event, thus potentially activating short-time scale processes (and thus also non-statistical events), while experiments are (more) in the statistical (or IVR) limit.

3. RESULTS

3.1 Pre-Dissociation Potential Energy Surface

As described above, HCO-Ala-NH_2 is a multifunctional molecule that can be protonated at various functional sites leading to several isomers. All structures (minima and transition states) and corresponding relative energies of the PES are reported in the Supporting Information (SI-C).

The full PES respect to barriers for proton transfer is reported in the Supporting Information (SI-D). Two of the most stable isomers, **AH4_a** and **AH2_a**, correspond to structures in which the proton is located in between the carbonyl groups. DFT results predict that the proton is moving from **AH4_a** (0.0 kJ/mol) to **AH2_a** (2.7 kJ/mol) through a small barrier **Ts1** that becomes barrierless when including zero point energy (-2.6 kJ/mol). This is confirmed by MP2 calculations where the transition state is also located at -0.2 kJ/mol from **AH2_a** (0.0 kJ/mol) and **AH4_a** (2.3 kJ/mol). This means that before any collision, experimentally, the system should shuttle between these two structures without any energy barrier. Therefore, ions detected in positive-ion mass spectra probably correspond to a mixture between both **AH4_a** and **AH2_a** structures. On the other hand, PM3 calculations provided a barrier of 61.6 kJ/mol. This means that using the PM3 Hamiltonian, starting from **AH4_a** and **AH2_a** structures, we will underestimate this proton transfer and PM3 dynamics before any collision will not show any proton shuttling between **AH4_a** and **AH2_a**. Differences between PM3 and B3LYP PES are not only confined in proton transfer. We discuss these differences based on comparison between PM3 and B3LYP dynamics results (see Section 3.4) and careful investigation of each reaction pathways (see Section 4). Here we can anticipate that from an empirical point of view PM3 seems to be suited to describe fragmentation reactivity, since results are in agreement with experiments and with B3LYP chemical dynamics, and that this is probably due to the fact that the exit channels are reasonably well reproduced (i.e. differences with B3LYP are smaller) and that barriers to exit channels are bigger than those corresponding to proton transfer. Finally, PM3, with the aforementione exception of the proton transfer between structures **AH4_a** and **AH2_a**, underestimates energy barriers with respect to B3LYP but the profiles are similar (i.e. they proceed, after a given point of difference, in an almost "parallel"

way) and thus we can consider that PM3 overestimates the reactivity expected from B3LYP calculations.

3.2. IRMPD Experiments

Before discussing fragmentation, we first report the results of IRMPD experiments that were performed in order to gain some insights about the structures that are most likely present in gas phase before collisions. Figure 3 shows the IRMPD spectrum of the protonated HCO-Ala-NH_2 recorded upon irradiation by the IR FEL in the 1300-1800 cm^{-1} energy range. Assignments of the experimental IR absorption spectrum is achieved by comparison with the IR spectra obtained from DFT for the structures used later in the simulation (**AH4_a**, **AH4_b**, **AH2_a**, **AH2_c**, **AH1** and **AH3**), For the sake of comparison, computed absorption cross-sections are represented in Figure 3 by assuming a Gaussian profile (fwhm=15 cm^{-1}) for each calculated infrared band. Experimental IRMPD spectra are obtained by plotting the photofragmentation yield R ($R= - \ln(I_P/(I_P + \Sigma I_F))$, where I_p is the intensity of the precursor ion and ΣI_F is the sum of the intensities of the fragment ions as a function of the IR radiation wavenumber. The fragmentation yield was about 20 % for $[(HCO\text{-}Ala\text{-}NH_2)H]^+$ using four IR-FEL macropulses, suggesting an excellent spatial overlap between the laser and the ion cloud and/or low threshold dissociation energies.[46] In the following, as far as the positions are concerned, all theoretical vibrational modes were scaled with a factor of 0.97 known to be appropriate for DFT calculations as suggested by Schlegel and coworkers. [57, 58]

The IRMPD spectrum of the protonated HCO-Ala-NH_2 is dominated by an intense broad band centered at ~1690 cm^{-1} that can be the superposition of both amide and formyl O=C symmetrical stretching modes, mainly from **AH2_a**, **AH2_c** and **AH4_a** . These suggest that the presence of an intramolecular hydrogen bond between both carbonyl groups induces a red-shift of their (its) stretching frequencies by about 80 cm^{-1}.[59] No experimental signals were detected above 1700 cm^{-1}, suggesting the lack of any "free" carbonyl group, whose stretching mode is detected around and above 1800 cm^{-1}, as observed for

instance for protonated nucleobases [60] or small peptides.[14] (More ref here?)Another band is detected at ~1600 cm^{-1} which may correspond to the NH_2 scissoring vibrational mode in **AH2_a**, **AH4_a** and **AH4_b**. It is also observed a small feature at ~1525 cm^{-1} that may be attributed to a the C-NH-C antisymmetrical stretching vibrational mode in **AH2_a**,**AH2_c**, **AH3** and **AH4_a**. The last broad band, detected experimentally around 1350 cm^{-1}, could correspond to a CH bending vibrational mode and it matches with both cyclic structures **AH2_a** and **AH4_a**. In summary, it turns out from IRMPD experiments that **AH2_a** and **AH4_a** seem to be the most probable structures generated by electrospray before the collision, thereby confirming DFT calculations that predict them as the most relevant in gas phase before collision.

3.3. Mass spectrometry and CID Experiments

Under the electrospray conditions used, the most abundant ion observed is the protonated peptide, detected at *m/z* 117, and at *m/z* 118 for both D- and ^{13}C-labeled peptides. The $[(HCO\text{-}Ala\text{-}NH_2)H]^+$ ion was then selected in order to record its MS/MS spectrum (Figure 4). In addition, the use of labeled compounds allows us providing insights on the fragmentation mechanisms associated with the formation of the various product ions. CID results obtained for both unlabeled and labeled compounds are summarized in Table 1.

As shown in Figure 4a, four dissociation channels were observed. The first one (*m/z* 100) corresponds to the loss of NH_3 (formation of b_1, Figure1). Another prominent peak is associated with the loss of carbon monoxide (formation of y_1). The use of ^{13}C-labeling unambiguously demonstrates that the labeled carbonyl group is specifically eliminated (loss of 29 Daltons). Furthermore, labeled compounds give useful information for the two remaining processes. Thus, both ^{13}C and deuterium atoms stay after fragmentation in the "a_1" fragment and consequently the [H_3, C, O, N] moiety eliminated (loss of 45 Daltons) does not include the formyl group. The last process gives rise to the *m/z* 44 immonium ion *I* through the loss of [H_3,C_2,O_2,N]. Examination of Figure 4b shows that with $(DCO\text{-}Ala\text{-}NH_2)$, this

particular process is characterized by two peaks at *m/z* 44 and 45. This indicates that there are at least two fragmentation pathways for the ***I*** formation. In one of them, hydrogen atom of the formyl group is eliminated within the neutral moiety.

3.4. Chemical dynamics simulations

We have performed direct dynamics simulations using the six most relevant structures as starting points, namely **AH4_a**, **AH4_b**, **AH2_a**, **AH2_c**, **AH1** and **AH3** (Figure 2). We can distinguish three types of reactivity yields: very low reactivity (2 –3 %) corresponding to initial structures in which the proton is located on the formyl group (structures **AH4_a** and **AH4_b**); medium reactivity (14 – 16 %) when the proton is on the amide carbonyl group (structures **AH2_a** and **AH2_c**); and finally higher reactivity for the less energetically favored structures, which are protonated onto one of the nitrogen atom (**AH1** and **AH3**). Details on reactivity yields obtained are reported in Supporting Information (SI-E). We should note that reactivity yields depend mainly on protonation site rather than on conformation. This is due to the fact that, prior to collision, thermal energy allows each isomer to rotate along dihedral angles, like those connecting **AH4_a** to **AH4_b** or **AH2_a** with **AH2_c**. Thus, pairs of structures with similar protonation sites (**AH4_a**/**AH4_b** and **AH2_a**/**AH2_c**) give similar reactivities.

In case of **AH4_a** and **AH2_a** structures, it is expected from B3LYP and MP2 PES results that before collision the proton should shuttle within the two carbonyl groups. On the other hand, PM3 provides a barrier for this proton transfer. Consequently, PM3 dynamics did not show any proton shuttling between both structures prior collision. This corresponds to the following: we simulate collisions for both **AH4_a** and **AH2_a**fixed protonation initial states as an approximation of the mixed state where the proton shuttles between the two sites. The reliability of this approximation is verified by comparing fragmentation results with experiments. We should further remark that B3LYP-based dynamics, based on a PES where the proton transfer is barrierless, did not show any such proton transfer prior collision either.

Theoretical MS/MS spectra obtained from chemical dynamic simulations for each initial geometries are reported in Supporting information (SI-F) and summarized in table 2. All the fragments observed experimentally (see Figure 4), b_1, y_1, a_1 and *I* ions, are also present in the spectra obtained by chemical dynamics simulations. Three fragments, a_1* (*m/z* 74), X_0 (*m/z* 46) and B_0 (*m/z* 29), are found in the theoretical MS/MS, at small quantity, but not observed experimentally.The a_1 (*m/z* 72) and *I* (*m/z* 44) experimental fragment ions are both observed in all of the theoretical MS/MS spectra. b_1 (loss of ammonia, *m/z* 100) and y_1 (loss of CO, *m/z* 89) fragment ions are obtained mainly when **AH1** and **AH3** isomers are used as initial structures, respectively, but also few trajectories leading to b_1 and y_1 fragments were found when starting from **AH4_a** and **AH4_b** isomers. Note that, as shown by the pre dissociation PES (Supporting information SI-D), to achieve both fragmentations, it is necessary to convert **AH4_a** and **AH4_b** into **AH1** and **AH3** via sequential proton transfers. To let the system span in a statistically relevant fashion along the full PES starting from stable **AH4_a** and **AH4_b** structures, one should carry out simulations of at least one order of magnitude longer duration (we have actually performed thousands of simulation in the 10-50 ps time length). A possible way to circumvent this brute force approach, is to observe what happens when we activate structures in the PES leading to high energy local minima. This is what we have done by performing chemical dynamics simulations with **AH1** or **AH3** as initial geometries.

As aforementioned, few trajectories were carried out at DTF level using **AH4_a** structure as initial geometry. They lead to the formation of the a_1 (*m/z* 72) fragment but nob$_1$ or y_1 fragments were observed. This is probably due to the limited number of trajectories and, mainly, to the shorter timelength (less than 1 ps) reachable by B3LYP-based dynamics. On the other hand, X_0 (*m/z* 46) and B_0 (*m/z* 29) fragments not recorded experimentally, but obtained in PM3-based dynamics, were also observed by B3LYP-based dynamics. This suggests that the observation of these fragments in chemical dynamics is not due to the use of the PM3 semiempirical Hamiltonian in simulations.

4. FRAGMENTATION PATHWAYS

In order to better understand the various fragmentation pathways, we will now examine in details each fragment ion obtained, by combining results of simulations with those of experiments. The fragmentation mechanisms of X_0 (*m/z* 46), B_0 (*m/z* 29) and a_1* (*m/z* 74), not observed experimentally, are reported in the supporting information (SI-G).

4.1 Ammonia loss (*m/z* 100).

From the analysis of all the chemical dynamics trajectories, it turns out that the loss of NH_3 mostly arises from **AH1** (87.9%), **AH4_a** (7.3%) and **AH4_b** (4.8%) initial structures. When the initial structure is **AH4_a** or **AH4_b**, the NH_3 loss is obtained through a proton transfer from the formyl group to the amide carbonyl. Then, following the mechanism and the energy profile shown in Figure 5 (an example is also given as a movie in the supporting information; b1.mpg), the formation of oxazolone ring (**B**) is obtained in near all the cases (92%) while in the remaining (8%) the final structure is linear (**A**). Note that while B3LYP and PM3 differ in providing the energy for the exit channels b1_B (corresponding to the low energy path detailed by Paisz et al. [REF], where NH3 loss and ring formation are concerted) and b1_A (corresponding to the high energy path observed in our chemical dynamics simulations where first NH3 is removed and then the ring closes), both methods report b1_B as lower in energy than b1_A.

With both labeled compounds, the observed *m/z* value was 101 (neutral loss of 17 Daltons). Consequently, the proton eliminated together with the terminal amino group does not come from the formyl group. These results are consistent with the proposed mechanism shown in Figure 5.

4.2 CO loss (*m/z* 89).

From chemical dynamics simulations results, two different mechanisms may be proposed for the CO loss leading to the y_1 ion, as reported in Figure 6. Elimination of carbon monoxide is observed almost exclusively from **AH3** (98.8 %), and to a very minor extent from **AH4_a** (0.6 %) and **AH4_b** (0.6 %) initial structures. For the simulations starting from **AH4_a** and **AH4_b**, a proton transfer between the formyl and the amide carbonyl group occurs first, forming an **AH2**-like structure; then a second proton transfer leads to **AH3**. Thus the cleavage of the bond denoted **Y** is made possible leading to y_1 fragment following two possible pathways: the CHO moiety dissociates and donates a proton (**A**) to the amide carbonyl (74.0%) or (**B**) to the terminal amino group (26.0%). In the supporting information we report two prototypical movies corresponding to these mechanisms (y1_A.mpg and y1_B.mpg respectively). These mechanisms are supported by experiments with ^{13}C and ^{2}H-labeled peptides. Remarkably, MS/MS spectrum of protonated DCO-Ala-NH_2 indicates that deuterium and not hydrogen is transferred to the secondary amine (pathway **A**) or to the amide carbonyl (pathway **B**) as shown by the shifted *m/z* 90. Moreover, $H^{13}CO$-Ala-NH_2experiments reveal that the formyl carbonyl group is exclusively eliminated (neutral loss of 29 Daltons).

4.3 [H_3, C, O, N] loss (*m/z* 72).

The fragmentation product corresponding to *m/z* 72 has been obtained in all simulations. Surprisingly, ten different pathways leading to this fragment have been found, but two of which were observed in 99 % of the reactive trajectories and are shown in Figure 7. When initial geometries are **AH4_a** and **AH4_b**, a proton transfer is first required. In 52% of all cases, the proton migrates towards amide carbonyl position forming an **AH2**-like structure, as shown by arrow **1** in the Figure 7. In the remaining simulations a proton moves to the terminal amino group, leading to **AH1**-like structures, as shown by arrow **2** in the same Figure 7. In the first reaction pathway (**1**), following the proton transfer a direct loss of (OH-C-NH_2) has been recorded, as also reported in a prototypical simulation movie (supporting information; a1_1.mpg).In the second mechanism (**2**), after the first proton transfer, two consecutive

losses of neutrals were observed, first ammonia and then carbon monoxide, as also shown in supporting information (movie a1_2.mpg). Remarkably, these two mechanisms are similar to those recorded from B3LYP-based chemical dynamics simulations. With both labeled compounds, the mass of the neutral fragment remains unchanged as compared to the unlabeled peptide (45 Daltons). Consequently, the neutral moiety does not incorporate the formyl group. This experimental finding is in agreement with both proposed mechanisms.

4.4 [H_3, C_2, O_2, N] loss (*m/z* 44).

The fragment ion detected experimentally at *m/z* 44 corresponds to the immonium ion. It has been obtained starting from the six structures as initial structure through two different pathways (Figure 7 and 8).

The first fragmentation pathway is summarized in the Figure 7. The proton is initially located onto the formyl group (**AH4**), then a proton transfer first occurs either (**1**) to the amide carbonyl (60%)generating **AH2**-like structure or (**2**) to the amide nitrogen (40%), leading to **AH1** structure, as for the *m/z* 72 formation previously described. Then, two bonds are consecutively broken, first the bond named X breaks and then the bond named Y does (loss of CHO). After Y bond cleavage, the group CHO leaves the molecule and a proton transfer occurs from the CHO to the NH.

The second fragmentation mechanism is reported in Figure 8. When the starting structure is **AH3** the fragmentation pathway starts with the cleavage of the Z bond followed by CHO dissociation. Then, two different pathways can occur, proton transfer from the CHO either to (**1**) to the amide carbonyl (72 %) followed by W bond cleavage (an example is shown in supporting information, I1_Sch5_A.mpg), or to (**2**) to the amide nitrogen (28 %) followed by two successive losses: firstly ammonia and then carbon monoxide.

These mechanisms observed during direct dynamic simulations are again supported by isotopically labeled experiments. Remarkably, MS/MS spectra recorded with the ^{13}C-labeled peptide exhibit a peak at *m/z* 44, indicating that the labeled formyl carbon atom is not retained in the ionic fragment, in agreement with both mechanisms proposed in Figure 8. More interesting are the deuterium-labeled experiments. If one carefully examines the mechanisms that occurred during direct dynamics simulations, it is observed that according to Scheme 4, the deuterium would be incorporated in the ionic fragment, while it is expelled according to the mechanisms depicted in Figure 8. This is perfectly consistent with experimental results, where both product ions (*m/z* 44 and 45) were observed in the MS/MS spectrum of protonated DCO-Ala-NH_2 (Figure 4b). Consequently, this suggests that both proposed mechanisms are experienced by the system while leading to the immonium ion (fragment *I*, *m/z* 44).

CONCLUSIONS

Protonated HCO-Ala-NH_2 has been synthesized and investigated by a combined chemical dynamics and MS/MS studies. It has been shown that the "mobile proton" model can be used in order to achieve a better understanding of the MS/MS process of protonated peptides. According to experimental and theoretical results, the added proton moves amongst the four protonation sites in HCO-Ala-NH_2. Moreover, the fragmentation process occurs mainly by charge-directed reactions.

Remarkably, all the experimental MS/MS fragments (loss of ammonia, loss of CO, a_1 and immonium formation) were successfully identified by using direct dynamic simulations. Furthermore, MS/MS of labeled peptides are in perfect agreement with the recorded fragmentation pathways for all the ions. We should note that the oxazolone structure we have identified was first proposed by Harrison [Ref JASMS 1995] and the first direct evidence pointed out by IRMPD [REF JACS 2005], and later confirmed and

discussed by works of Maitre, Paisz and co-workers [Ref 59-61 of submitted paper] and Oomens, Polfer and co-workers [Refs 62-66 of submitted paper].

Notably, the use of a simple and approximated semi-empirical Hamiltonian for dynamics (PM3) – that is compulsory at the present time to perform a correct statistical sampling for such relatively large system – turned to be appropriate in supplying a qualitative explanation of the observed reactivity. From the comparison between DFT and PM3 PES, we can ground that on the fact that the energy barriers for dissociation are higher in energy than other those for proton transfer and that they regulate the reactivity. It resulted that, while part of the PES are quite different, two aspects suggest that PM3 dynamics is qualitatively instructive to complete the understanding of CID chemistry: (i) the exit channels (or transition states leading to a pre-dissociation) are higher in energy with respect to barriers for proton transfer (as previously found by Paisz et al. [**REF**]) and differences between PM3 and DFT are smaller in that part of the PES; (ii) even if a difference between PM3 and DFT is present and it can be also important in some region, the two surfaces are 'almost' parallel, i.e. they do not cross (except one case where the energy difference is small). We can further suggest that, since PM3 barriers are sistematically lower than DFT ones in the regions that determine the final fragmentation products, we overestimate reactivity at a given energy, such that what we observe can be reported to higher values of really transferred energy.

Finally, the QM+MM direct dynamics simulations of protonated CID was shown to provide a complementary picture of the M/MS fragmentation processes and rationalize experimental findings.

ANKNOWLEDGEMENTS

We thank M-P. Gaigeot for useful discussions. KS thanks UEVE for a visiting fellowship and partial support from the Basic Science Program through the National Research Foundation of Korea (KRF) administered by the Ministry of Education, Science and Technology (2012-0002654). DO and JYS thank the CLIO team (J. M. Ortega, C. Six, G. Perilhous, J. P. Berthet) as well as P. Maître, V.

Steinmetz and O. Hernandez for their support during the experiments.This work was granted access to the HPC resources of CCRT under the allocation 2012082123 made by GENCI (Grand Equipement National de Calcul Intensif).AR and PMG thank the Spanish *Ministerio de Economia y Competitividad* (CTQ2011-23620), the *Generalitat de Catalunya* (2009SGR 00901) and IRB Barcelona for financial support.

REFERENCES

[1] R. Aebersold, D.R. Goodlett, Mass spectrometry in proteomics, Chem. Rev., 101 (2001) 269-295.
[2] K. Biemann, Contributions of mass spectrometry to peptide and protein structure, Biomed. Environ. Mass, 16 (1988) 99-111.
[3] P. Roepstorff, J. Fohlman, Proposal for a common nomenclature for sequence ions in mass spectra of peptides, Biomed Mass Spectrom, 11 (1984) 601-601.
[4] I.V. Chernushevich, A.V. Loboda, B.A. Thomson, An introduction to quadrupole-time-of-flight mass spectrometry, J. Mass Spectrom., 36 (2001) 849-865.
[5] D.N. Perkins, D.J.C. Pappin, D.M. Creasy, J.S. Cottrell, Probability-based protein identification by searching sequence databases using mass spectrometry data, Electrophoresis, 20 (1999) 3551-3567.
[6] A.R. Dongre, J.K. Eng, J.R. Yates, Emerging tandem-mass-spectrometry techniques for the rapid identification of proteins, Trends in Biotechnology, 15 (1997) 418-425.
[7] R. Craig, R.C. Beavis, TANDEM: matching proteins with tandem mass spectra, Bioinformatics, 20 (2004) 1466-1467.
[8] B.J. Bythell, D.F. Barofsky, F. Pingitore, M.J. Polce, P. Wang, C. Wesdemiotis, B. Paizs, Backbone cleavages of carbon monoxide and sequential loss and ammonia from protonated AGG: A combined tandem mass spectrometry, isotope labeling, and theoretical study, J. Am. Soc. Mass Spectrom., 18 (2007) 1291-1303.
[9] M.M. Cordero, J.J. Houser, C. Wesdemiotis, Neutral products formed during backbone fragmentations of protonated peptides in tandem mass spectrometry, Anal. Chem., 65 (1993) 1594-1601.
[10] I.A. Papayannopoulos, The interpretation of collision-induced Dissociation tandem Mass-Spectra of peptides, Mass Spectrom. Rev., 14 (1995) 49-73.
[11] F. Pingitore, M.J. Polce, P. Wang, C. Wesdemiotis, B. Paizs, Intramolecular condensation reactions in protonated dipeptides: Carbon monoxide, water, and ammonia losses in competition, J. Am. Soc. Mass Spectrom., 15 (2004) 1025-1038.
[12] M.J. Polce, D. Ren, C. Wesdemiotis, Special feature: Commentary - Dissociation of the peptide bond in protonated peptides, J. Mass Spectrom., 35 (2000) 1391-1398.
[13] T. Yalcin, I.G. Csizmadia, M.R. Peterson, A.G. Harrison, The structure and fragmentation of B-n (n>=3) ions in peptide spectra, J. Am. Soc. Mass Spectrom., 7 (1996) 233-242.
[14] B.J. Bythell, P. Maitre, B. Paizs, Cyclization and Rearrangement Reactions of a(n) Fragment Ions of Protonated Peptides, J. Am. Chem. Soc., 132 (2010) 14766-14779.
[15] D.M. Good, C. Marin-Vicente, R.A. Zubarev, Are the majority of a(2)-ions cyclic?, Phys. Chem. Chem. Phys, 12 (2010) 13372-13374.
[16] B. Balta, V. Aviyente, C. Lifshitz, Elimination of water from the carboxyl group of GlyGlyH(+), J. Am. Soc. Mass Spectrom., 14 (2003) 1192-1203.

[17] G.E. Reid, R.J. Simpson, R.A.J. O'Hair, A mass spectrometric and ab initio study of the pathways for dehydration of simple glycine and cysteine-containing peptide M+H (+) ions, J. Am. Soc. Mass Spectrom., 9 (1998) 945-956.
[18] B. Paizs, I.P. Csonka, G. Lendvay, S. Suhai, Proton mobility in protonated glycylglycine and N-formylglycylglycinamide: a combined quantum chemical and RKKM study, Rapid Commun. Mass Spectrom., 15 (2001) 637-650.
[19] B. Paizs, S. Suhai, Theoretical study of the main fragmentation pathways for protonated glycylglycine, Rapid Commun. Mass Spectrom., 15 (2001) 651-663.
[20] B. Paizs, Z. Szlavik, G. Lendvay, K. Vekey, S. Suhai, Formation of a(2)(+) ions of protonated peptides. An ab initio study, Rapid Commun. Mass Spectrom., 14 (2000) 746-755.
[21] B. Paizs, G. Lendvay, K. Vekey, S. Suhai, Formation of b(2)(+) ions from protonated peptides: an ab initio study, Rapid Commun. Mass Spectrom., 13 (1999) 525-533.
[22] T. Yalcin, C. Khouw, I.G. Csizmadia, M.R. Peterson, A.G. Harrison, Why are B ions stable species in peptide spectra?, J. Am. Soc. Mass Spectrom., 6 (1995) 1165-1174.
[23] N.C. Polfer, J. Oomens, S. Suhai, B. Paizs, Spectroscopic and theoretical evidence for oxazolone ring formation in collision-induced dissociation of peptides, J. Am. Chem. Soc., 127 (2005) 17154-17155.
[24] I. Komaromi, A. Somogyi, V.H. Wysocki, Proton migration and its effect on the MS fragmentation of N-acetyl OMe proline: MS/MS experiments and ab initio and density functional calculations, Int. J. Mass Spectrom., 241 (2005) 315-323.
[25] A.G. Harrison, A.B. Young, C. Bleiholder, S. Suhai, B. Paizs, Scrambling of sequence information in collision-induced dissociation of peptides, J. Am. Chem. Soc., 128 (2006) 10364-10365.
[26] R.A.J. O'Hair, M.L. Styles, G.E. Reid, Role of the sulfhydryl group on the gas phase fragmentation reactions of protonated cysteine and cysteine containing peptides, J. Am. Soc. Mass Spectrom., 9 (1998) 1275-1284.
[27] K.A. Cox, S.J. Gaskell, M. Morris, A. Whiting, Role of the site of protonation in the low-energy decompositions of gas phase peptide ions (vol 7, pg 522, 1996), J. Am. Soc. Mass Spectrom., 7 (1996) 759-759.
[28] I.P. Csonka, B. Paizs, G. Lendvay, S. Suhai, Proton mobility and main fragmentation pathways of protonated lysylglycine, Rapid Commun. Mass Spectrom., 15 (2001) 1457-1472.
[29] A.R. Dongre, J.L. Jones, A. Somogyi, V.H. Wysocki, Influence of peptide composition, gas-phase basicity, and chemical modification on fragmentation efficiency: Evidence for the mobile proton model, J. Am. Chem. Soc., 118 (1996) 8365-8374.
[30] A.G. Harrison, T. Yalcin, Proton mobility in protonated amino acids and peptides, Int. J. Mass Spectrom., 165 (1997) 339-347.
[31] V.H. Wysocki, G. Tsaprailis, L.L. Smith, L.A. Breci, Special feature: Commentary - Mobile and localized protons: a framework for understanding peptide dissociation, J. Mass Spectrom., 35 (2000) 1399-1406.
[32] I.P. Csonka, B. Paizs, G. Lendvay, S. Suhai, Proton mobility in protonated peptides: a joint molecular orbital and RRKM study, Rapid Commun. Mass Spectrom., 14 (2000) 417-431.
[33] R.C. Spezia, A.; Gaigeot, M-P.; Salpin, J-Y.; Song, K.; Hase, W.L., Collision Induced Dissociation of Doubly-charged Ions : Coulomb Explosion vs Neutral Loss in [Ca(urea)]2+ Gas Phase Unimolecular Reactivity via Chemical Dynamics Simulations, Phys. Chem. Chem. Phys, DOI:10.1039/C2CP41379E (2012).
[34] K. Park, B. Deb, K. Song, W.L. Hase, Importance of Shattering Fragmentation in the Surface-Induced Dissociation of Protonated Octaglycine, J. Am. Soc. Mass Spectrom., 20 (2009) 939-948.
[35] S.O. Meroueh, Y.F. Wang, W.L. Hase, Direct dynamics Simulations of collision- and surface-induced dissociation of N-protonated glycine. Shattering fragmentation, J. Phys. Chem. A, 106 (2002) 9983-9992.

[36] Y. Jeanvoine, M.-P. Gaigeot, W.L. Hase, K. Song, R. Spezia, Collision induced dissociation of protonated urea with N(2): Effects of rotational energy on reactivity and energy transfer via chemical dynamics simulations, Int. J. Mass Spectrom., 308 (2011) 289-298.
[37] R. Spezia, J.-Y. Salpin, M.-P. Gaigeot, W.L. Hase, K. Song, Protonated Urea Collision-Induced Dissociation. Comparison of Experiments and Chemical Dynamics Simulations, J. Phys. Chem. A, 113 (2009) 13853-13862.
[38] O. Meroueh, W.L. Hase, Collisional activation of small peptides, J. Phys. Chem. A, 103 (1999) 3981-3990.
[39] E. Martinez-Nunez, S.A. Vazquez, J.M.C. Marques, Quasiclassical trajectory study of the collision-induced dissociation of CH3SH++Ar, J. Chem. Phys., 121 (2004) 2571-2577.
[40] E. Martinez-Nunez, S.A. Vazquez, F.J. Aoiz, J.F. Castillo, Quasiclassical trajectory study of the collision-induced dissociation dynamics of Ar+CH3SH+ using an ab initio interpolated potential energy surface, J. Phys. Chem. A, 110 (2006) 1225-1231.
[41] E. Martinez-Nunez, A. Fernandez-Ramos, S.A. Vazquez, J.M.C. Marques, M.Y. Xue, W.L. Hase, Quasiclassical dynamics simulation of the collision-induced dissociation of Cr(CO)(6)(+) with Xe, J. Chem. Phys., 123 (2005).
[42] J.B. Liu, K. Song, W.L. Hase, S.L. Anderson, Direct dynamics study of energy transfer and collision-induced dissociation: Effects of impact energy, geometry, and reactant vibrational mode in H2CO+-Ne collisions, J. Chem. Phys., 119 (2003) 3040-3050.
[43] I. Corral, O. Mo, M. Yanez, J.-Y. Salpin, J. Tortajada, D. Moran, L. Radom, An experimental and theoretical investigation of gas-phase reactions of Ca2+ with glycine, Chem. Eur. J., 12 (2006) 6787-6796.
[44] A. Eizaguirre, O. Mo, M. Yanez, J.-Y. Salpin, Modeling the interactions between peptide functions and Sr(2+): formamide-Sr(2+) reactions in the gas phase, Phys. Chem. Chem. Phys, 13 (2011) 18409-18417.
[45] A.M. Lamsabhi, M. Alcami, O. Mo, M. Yanez, J. Tortajada, J.-Y. Salpin, Unimolecular reactivity of uracil-Cu2(+) complexes in the gas phase, ChemPhysChem, 8 (2007) 181-187.
[46] L. Mac Aleese, A. Simon, T.B. McMahon, J.M. Ortega, D. Scuderi, J. Lemaire, P. Maitre, Mid-IR spectroscopy of protonated leucine methyl ester performed with an FTICR or a Paul type ion-trap, Int. J. Mass Spectrom., 249 (2006) 14-20.
[47] R. Prazeres, F. Glotin, C. Insa, D.A. Jaroszynski, J.M. Ortega, Two-colour operation of a Free-Electron Laser and applications in the mid-infrared, Eur. Phys. J. D., 3 (1998) 87-93.
[48] A.D. Becke, A new mixing of Hartree–Fock and local density-functional theories, J. Chem. Phys., 98 (1993) 1372-1377.
[49] C.T. Lee, W.T. Yang, R.G. Parr, Development of the Colle-Salvetti correlation-energy formula into a functional of the electron density, Phys. Rev. B, 37 (1988) 785-789.
[50] M.J. Frisch, G.W. Trucks, H.B. Schlegel, G.E. Scuseria, M.A. Robb, J.R. Cheeseman, J. Montgomery, J. A.;, T. Vreven, K.N. Kudin, J.C. Burant, J.M. Millam, S.S. Iyengar, J. Tomasi, V. Barone, B. Mennucci, M. Cossi, G. Scalmani, N. Rega, G.A. Petersson, H. Nakatsuji, M. Hada, M. Ehara, K. Toyota, R. Fukuda, J. Hasegawa, M. Ishida, T. Nakajima, Y. Honda, O. Kitao, H. Nakai, M. Klene, X. Li, J.E. Knox, H.P. Hratchian, J.B. Cross, V. Bakken, C. Adamo, J. Jaramillo, R. Gomperts, R.E. Stratmann, O. Yazyev, A.J. Austin, R. Cammi, C. Pomelli, J.W. Ochterski, P.Y. Ayala, K. Morokuma, G.A. Voth, P. Salvador, J.J. Dannenberg, V.G. Zakrzewski, S. Dapprich, A.D. Daniels, M.C. Strain, O. Farkas, D.K. Malick, A.D. Rabuck, K. Raghavachari, J.B. Foresman, J.V. Ortiz, Q. Cui, A.G. Baboul, S. Clifford, J. Cioslowski, B.B. Stefanov, G. Liu, A. Liashenko, P. Piskorz, I. Komaromi, R.L. Martin, D.J. Fox, T. Keith, M.A. Al-Laham, C.Y. Peng, A. Nanayakkara, M. Challacombe, P.M.W. Gill, B. Johnson, W. Chen, M.W. Wong, C. Gonzalez, J.A. Pople, Gaussian Program Suite, in: Gaussian 03, Gaussian, Inc., Wallingford,CT, 2004.
[51] S. Chapman, D.L. Bunker, An exploratory study of reactant vibrational effects in CH3 + H2 and its isotopic variants, J. Chem. Phys., 62 (1975) 2890-2899.

[52] W.L. Hase, Y.J. Cho, Trajectory studies of S(N)2 nucleophilic substitution. 3. Dynamic stereochemistry and energy-transfer pathways for the Cl-+CH3Cl association and direct substitution-reactions, J. Chem. Phys., 98 (1993) 8626-8639.
[53] C.S. Sloane, W.L. Hase, On the dynamics of state selected unimolecular reactions: Chloroacetylene dissociation and predissociation, J. Chem. Phys., 66 (1977) 1523-1533.
[54] X.C. Hu, W.L. Hase, T. Pirraglia, Vectorization of the General Monte Carlo Classical Trajectory Program VENUS, J. Comput. Chem., 12 (1991) 1014-1024.
[55] W.L. Hase, Duchovic, R,J.; Hu, X.; Komornicki, A.; Lim, K.;Lu, D-H.; Peslherbe, G.H.; Swamy, K.N.; Vande Linde, S.R.; Wang, H.;Wolf, R.J., VENUS96, a General Chemical Dynamics Computer Program, QCPE, 16 (1996).
[56] J.J.P. Stewart, Special Issue -MOPAC- A semiempirical molecular-orbital program, J. Comput.-Aided Mol. Des., 4 (1990) 1-45.
[57] M.D. Halls, H.B. Schlegel, Comparison of the performance of local, gradient-corrected, and hybrid density functional models in predicting infrared intensities, J. Chem. Phys., 109 (1998) 10587-10593.
[58] M.D. Halls, J. Velkovski, H.B. Schlegel, Harmonic frequency scaling factors for Hartree-Fock, S-VWN, B-LYP, B3-LYP, B3-PW91 and MP2 with the Sadlej pVTZ electric property basis set, Theoret. Chem. Acc., 105 (2001) 413-421.
[59] B. Lucas, G. Gregoire, J. Lemaire, P. Maitre, J.M. Ortega, A. Rupenyan, B. Reimann, J.P. Schermann, C. Desfrancois, Investigation of the protonation site in the dialanine peptide by infrared multiphoton dissociation spectroscopy, Phys. Chem. Chem. Phys, 6 (2004) 2659-2663.
[60] J.Y. Salpin, S. Guillaumont, J. Tortajada, L. MacAleese, J. Lemaire, P. Maitre, Infrared spectra of protonated uracil, thymine and cytosine, ChemPhysChem, 8 (2007) 2235-2244.
[61] B. Paizs, B.J. Bythell, P. Maitre, Rearrangement Pathways of the a(4) Ion of Protonated YGGFL Characterized by IR Spectroscopy and Modeling, J. Am. Soc. Mass Spectrom., 23 (2012) 664-675.
[62] R.K. Sinha, U. Erlekam, B.J. Bythell, B. Paizs, P. Maitre, Diagnosing the Protonation Site of b (2) Peptide Fragment Ions using IRMPD in the X-H (X = O, N, and C) Stretching Region, J. Am. Soc. Mass Spectrom., 22 (2011) 1645-1650.
[63] U. Erlekam, B.J. Bythell, D. Scuderi, M. Van Stipdonk, B. Paizs, P. Maitre, Infrared Spectroscopy of Fragments of Protonated Peptides: Direct Evidence for Macrocyclic Structures of b(5) Ions, J. Am. Chem. Soc., 131 (2009) 11503-11508.
[64] X. Chen, L. Yu, J.D. Steill, J. Oomens, N.C. Polfer, Effect of Peptide Fragment Size on the Propensity of Cyclization in Collision-Induced Dissociation: Oligoglycine b(2)-b(8), J. Am. Chem. Soc., 131 (2009) 18272-18282.
[65] J. Grzetic, J. Oomens, Spectroscopic Evidence for an Oxazolone Structure in Anionic b-Type Peptide Fragments, J. Am. Soc. Mass Spectrom., 23 (2012) 290-300.
[66] M.J. Kullman, S. Molesworth, G. Berden, J. Oomens, M. Van Stipdonk, IRMPD spectroscopy b(2) ions from protonated tripeptides with 4-aminomethyl benzoic acid residues, Int. J. Mass Spectrom., 316 (2012) 174-181.
[67] M. Tirado, J. Rutters, X. Chen, A. Yeung, J. van Maarseveen, J.R. Eyler, G. Berden, J. Oomens, N.C. Polfer, Disfavoring Macrocycle b Fragments by Constraining Torsional Freedom: The "Twisted" Case of QWFGLM b(6), J. Am. Soc. Mass Spectrom., 23 (2012) 475-482.
[68] S. Zou, J. Oomens, N.C. Polfer, Competition between diketopiperazine and oxazolone formation in water loss products from protonated ArgGly and GlyArg, Int. J. Mass Spectrom., 316 (2012) 12-17.

FIGURE AND TABLE CAPTIONS

Figure 1: Sequence ions in (HCO-Ala-NH_2) following the peptide fragmentation nomenclature.[3] Red numbers show the different protonation sites taken into account, namely amide nitrogen (1), amide carbonyl (2), amide nitrogen (3) and formyl group (4).

Figure 2: Optimized structures for protonated (HCO-Ala-NH_2). Energies, in parenthesis, are in kJ/mol.

Figure 3: Experimental IRMPD a) and theoretical IR spectra b-g) of $[(HCO\text{-}Ala\text{-}NH_2)H]^+$. Calculations are carried out at the B3LYP/6-311++G(d,p) level of theory. The experimental spectrum of panel a is superimposed in light gray over each theoretical spectrum.

Figure 4: Energy profile associated for dissociation mechanism for formation of b_1 ion. It was calculated at B3LYP/6-311++G(2df,2p)//B3LYP/6-311++G(d,p)+ZPE level (in black and continuous profile) and PM3 level (in green and non-continuous profile).

Figure 5: Energy profile associated for dissociation mechanism for formation of y_1 ion. The numbers on the arrows represent the proton transfer from CHO moiety to the (1) amide carbonyl and (2) secondary amine. It was calculated at B3LYP/6-311++G(2df,2p)//B3LYP/6-311++G(d,p)+ZPE level (in black and continuous profile) and PM3 level (in green and non-continuous profile).

Figure 6: Energy profile associated for dissociation mechanism for formation of a_1 and *I* ions. The numbers on the arrows represent the proton transfer from the formyl group to the (1) amide carbonyl and (2) amide nitrogen. It was calculated at B3LYP/6-311++G(2df,2p)//B3LYP/6-311++G(d,p)+ZPE level (in black and continuous profile) and PM3 level (in green and non-continuous profile).

Figure 7: Energy profile associated for dissociation mechanism for formation of *I* ion. The numbers on the arrows represent the proton transfer from the formyl group to the (1) amide carbonyl and (2) amide nitrogen. It was calculated at B3LYP/6-311++G(2df,2p)//B3LYP/6-311++G(d,p)+ZPE level (in black and continuous profile) and PM3 level (in green and non-continuous profile).

Table 1: Product ions observed experimentally during the fragmentation of protonated HCO-Ala-NH_2.

Table 2: Comparison between both theoretical and experimental MS/MS depending on the starting structure of protonated HCO-Ala-NH_2.

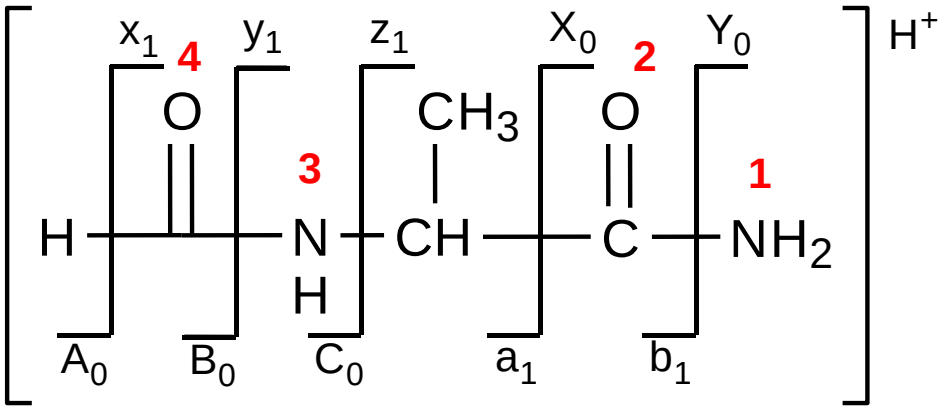

Figure 1

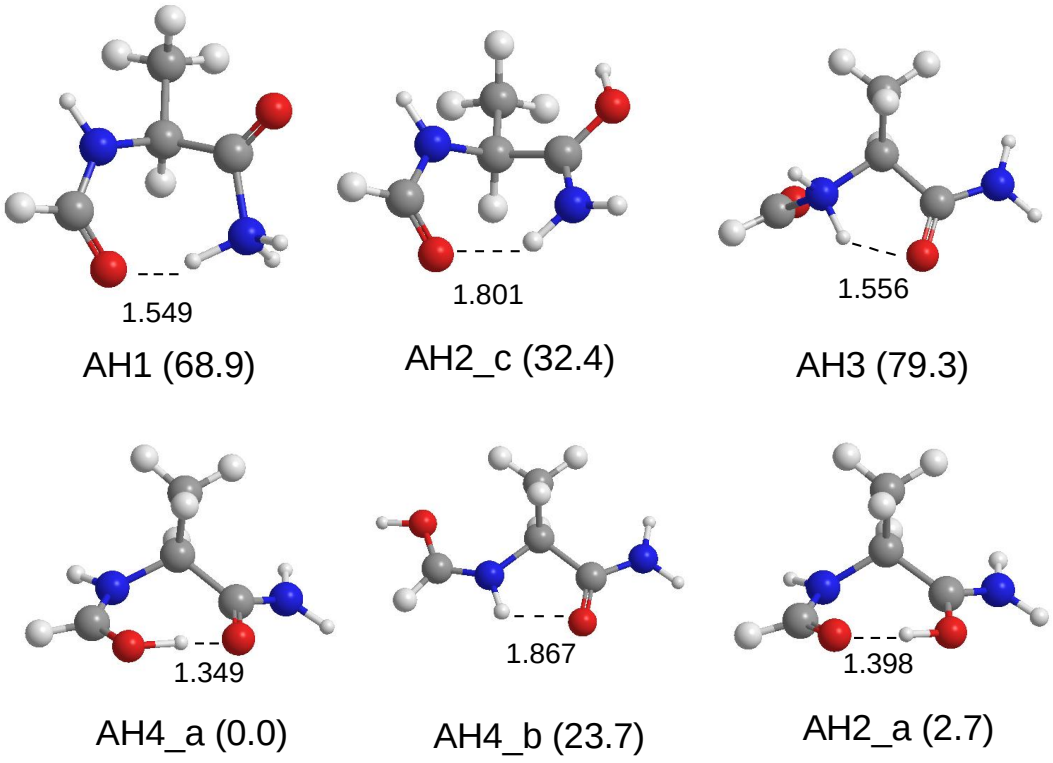
1.549
AH1 (68.9)
1.801
AH2_c (32.4)
1.556
AH3 (79.3)
1.349
AH4_a (0.0)
1.867
AH4_b (23.7)
1.398
AH2_a (2.7)

Figure 2

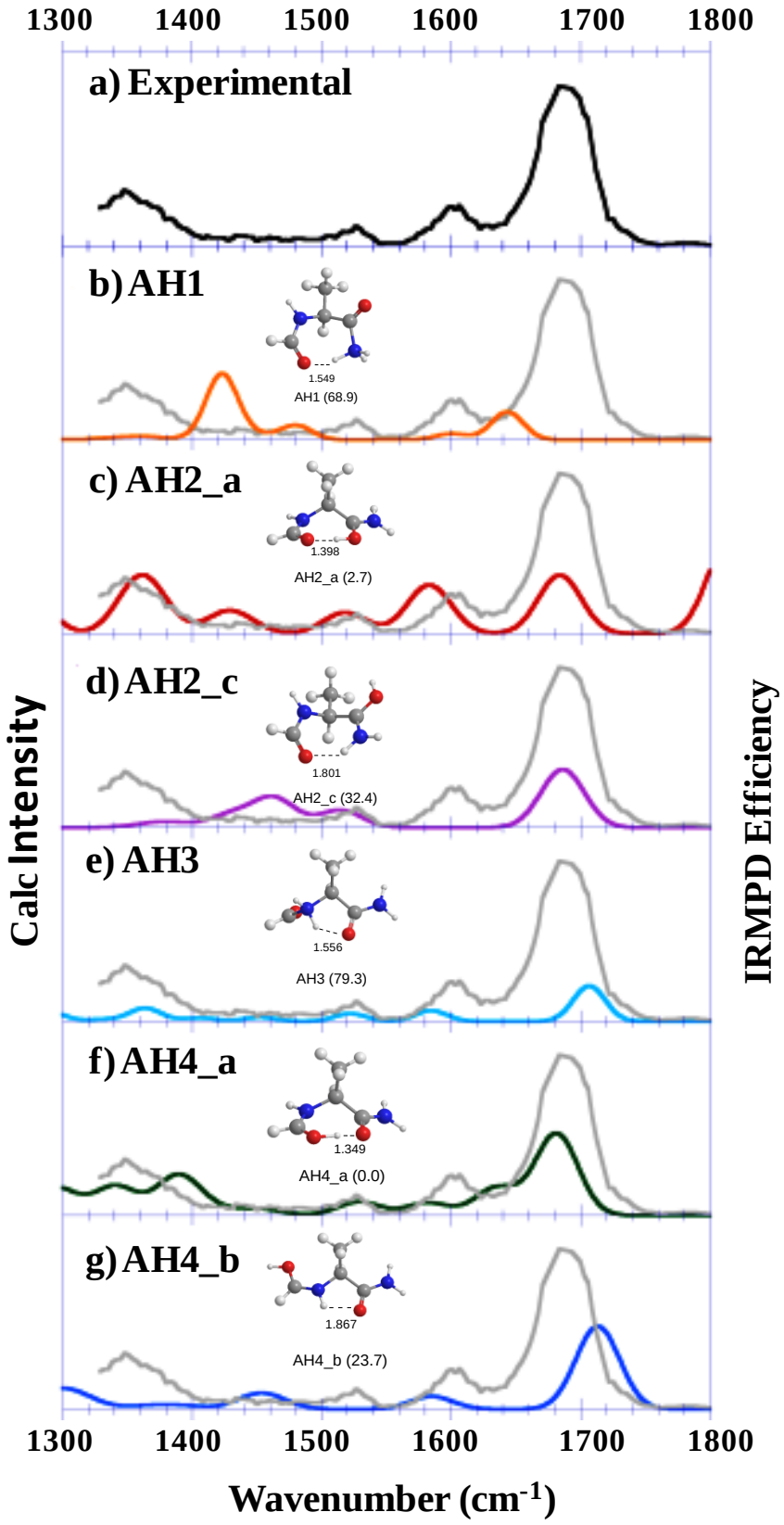
1300
1400
1500
1600
1700
1800
a) Experimental
b) AH1
1.549
AH1 (68.9)
c) AH2_a
1.398
AH2_a (2.7)
d) AH2_c
1.801
AH2_c (32.4)
e) AH3
1.556
AH3 (79.3)
f) AH4_a
1.349
AH4_a (0.0)
g) AH4_b
1.867
AH4_b (23.7)
Calc Intensity
IRMPD Efficiency
Wavenumber (cm-1)

Figure 3

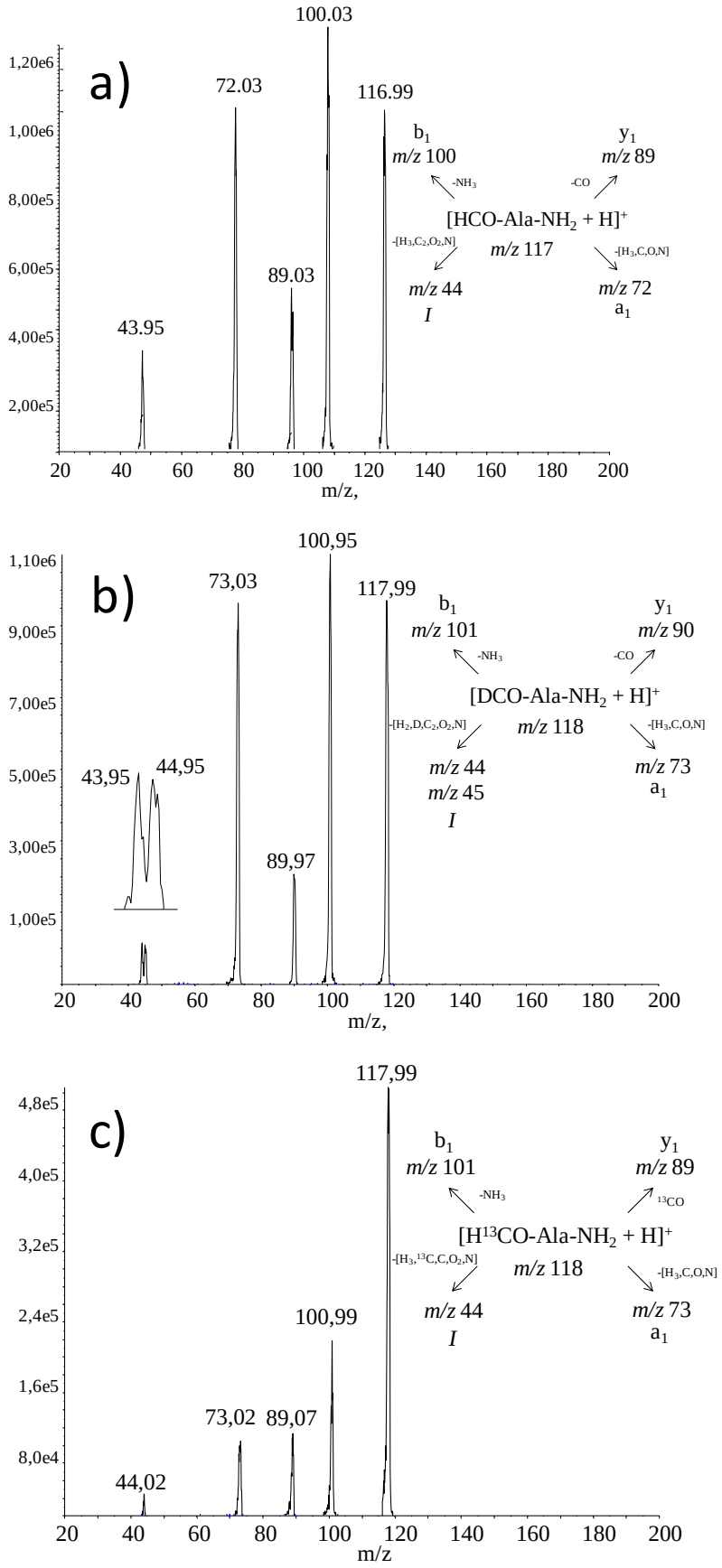
a)
100.03
72.03
116.99
89.03
43.95
b1
m/z 100
y1
m/z 89
-NH3
-CO
[HCO-Ala-NH2 + H]+
m/z 117
-[H3,C2,O2,N]
-[H3,C,O,N]
m/z 44
I
m/z 72
a1
1,20e6
1,00e6
8,00e5
6,00e5
4,00e5
2,00e5
20 40 60 80 100 120 140 160 180 200
m/z,
b)
100,95
73,03
117,99
89,97
43,95
44,95
b1
m/z 101
y1
m/z 90
-NH3
-CO
[DCO-Ala-NH2 + H]+
m/z 118
-[H2,D,C2,O2,N]
-[H3,C,O,N]
m/z 44
m/z 45
I
m/z 73
a1
1,10e6
9,00e5
7,00e5
5,00e5
3,00e5
1,00e5
20 40 60 80 100 120 140 160 180 200
m/z,
c)
117,99
100,99
73,02
89,07
44,02
b1
m/z 101
y1
m/z 89
-NH3
13CO
[H13CO-Ala-NH2 + H]+
m/z 118
-[H3,13C,C,O2,N]
-[H3,C,O,N]
m/z 44
I
m/z 73
a1
4,8e5
4,0e5
3,2e5
2,4e5
1,6e5
8,0e4
20 40 60 80 100 120 140 160 180 200
m/z

Figure 4

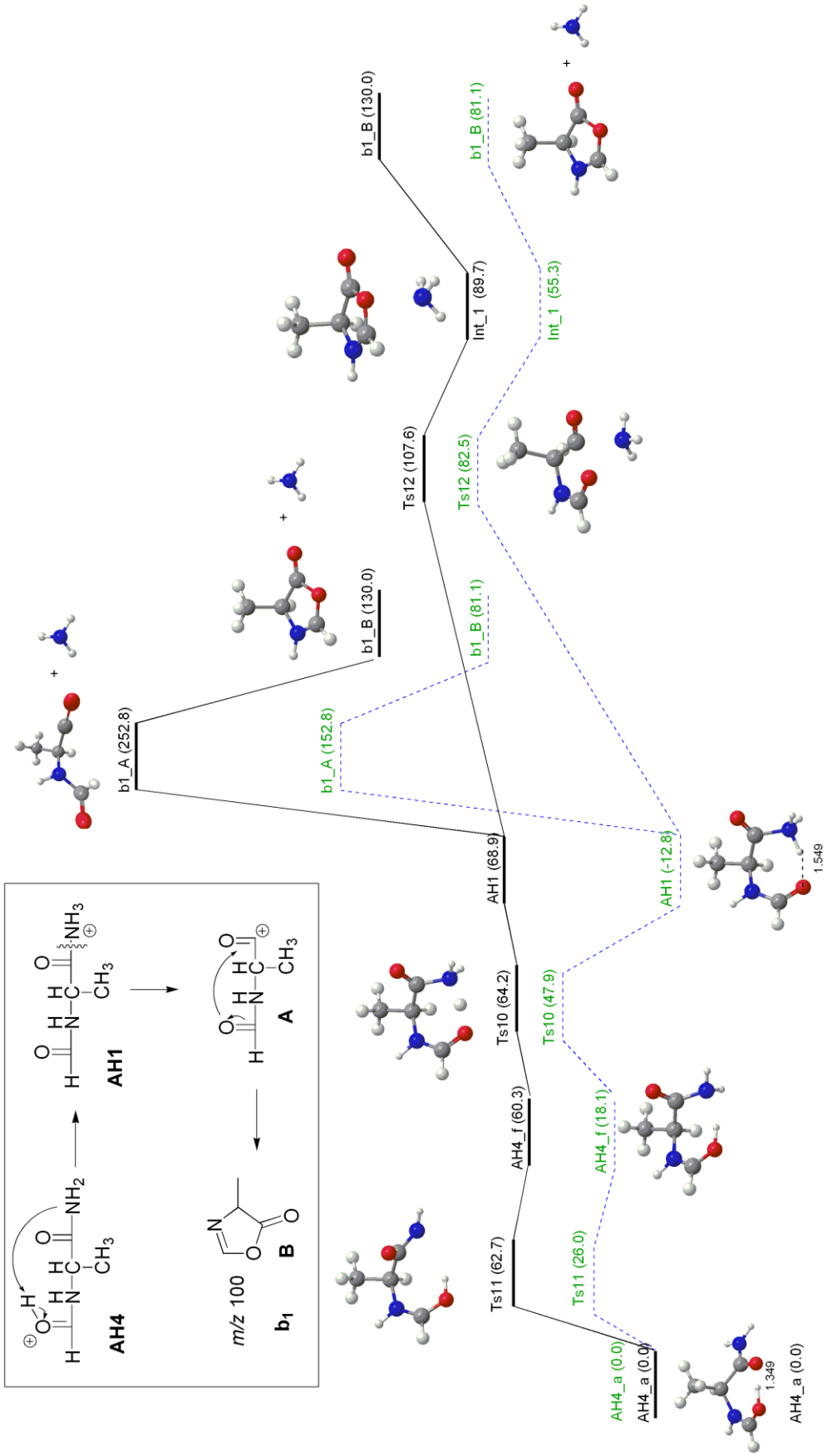
AH4
AH1
A
B
b1
m/z 100
b1_A (252.8)
b1_B (130.0)
Ts12 (107.6)
Int_1 (89.7)
b1_B (130.0)
b1_A (152.8)
b1_B (81.1)
Ts12 (82.5)
Int_1 (55.3)
b1_B (81.1)
AH1 (68.9)
AH1 (-12.8)
Ts10 (64.2)
Ts10 (47.9)
AH4_f (60.3)
AH4_f (18.1)
Ts11 (62.7)
Ts11 (26.0)
AH4_a (0.0)
AH4_a (0.0)
AH4_a (0.0)
1.549
1.349

Figure 5

AH4
AH2
AH3
y1
m/z 89
A
B
Path 1
Path 2
Path 1
Path 2
AH4_a (0.0)
Ts1 (33.8)
AH2_a (2.7)
Ts1 (-2.6)
Ts4 (44.7)
AH2_c (32.4)
Ts5 (48.6)
AH2_d (35.2)
Ts6 (74.6)
AH3 (79.3)
Ts13 (129.6)
y1_A (53.1)
Int_2(46.7)
Ts14 (134.2)
y1_B (40.8)
Int_3 (21.8)
AH4_a (0.0)
Ts1 (33.8)
AH2_a (-23.8)
Ts4 (-16.2)
AH2_c (-27.8)
Ts5 (-16.2)
AH2_d (-24.3)
Ts6 (60.3)
AH3 (19.6)
Ts13 (64.3)
y1_A (33.0)
Int_2 (-12.5)
Ts14 (107.3)
y1_B (24.3)
Int_3 (-20.4)
1.256
1.349
1.398
1.801
1.394
1.556

Figure 6

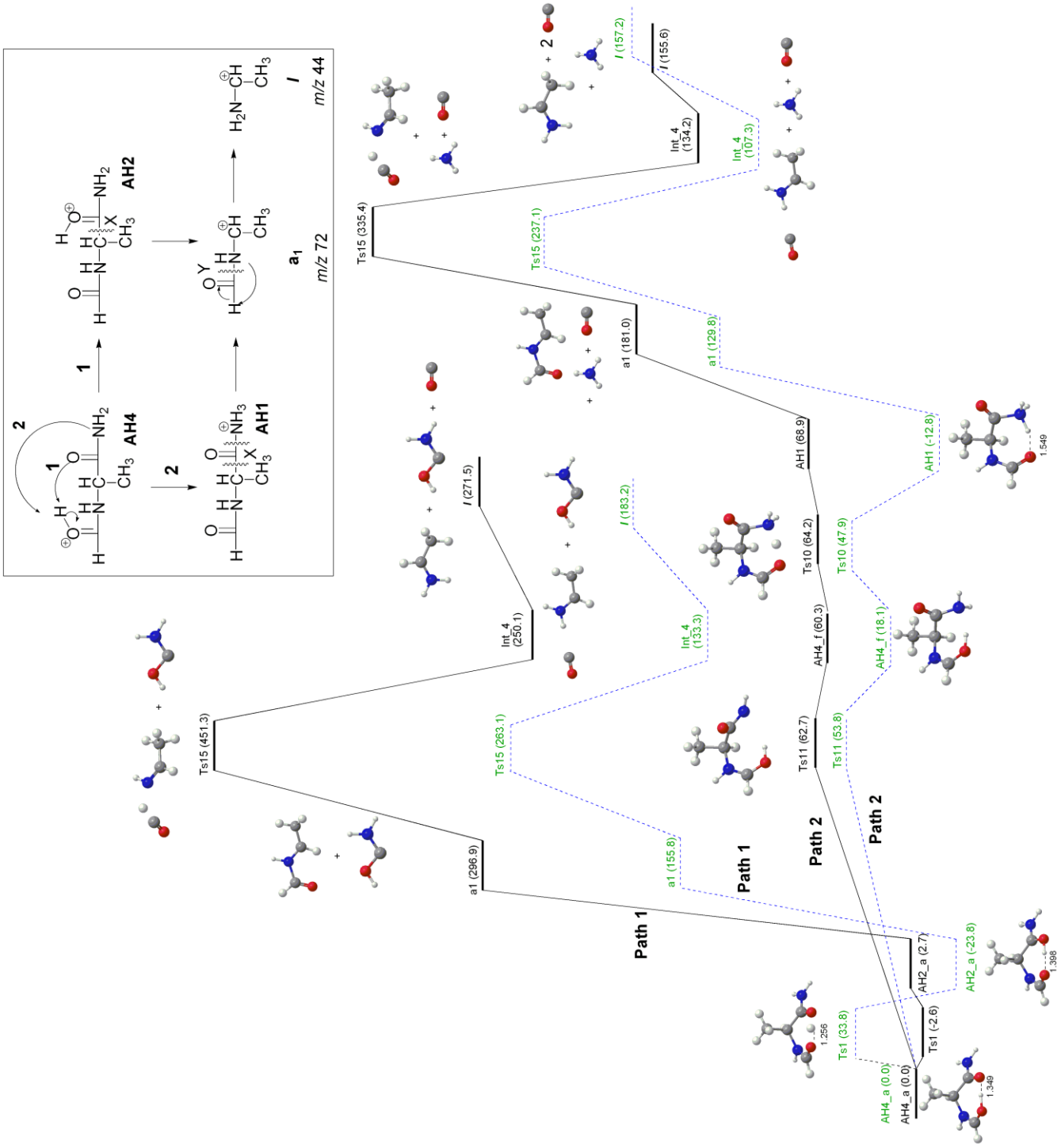
AH4
AH2
AH1
I
m/z 44
a1
m/z 72
Ts15 (451.3)
a1 (296.9)
Int_4 (250.1)
I (271.5)
Ts15 (263.1)
a1 (155.8)
Int_4 (133.3)
I (183.2)
Ts15 (335.4)
a1 (181.0)
Int_4 (134.2)
I (155.6)
Ts15 (237.1)
a1 (129.8)
Int_4 (107.3)
I (157.2)
AH4_a (0.0)
Ts1 (33.8)
AH4_a (0.0)
Ts1 (-2.6)
AH2_a (2.7)
AH2_a (-23.8)
AH4_f (60.3)
Ts11 (62.7)
Ts11 (53.8)
AH4_f (18.1)
AH1 (68.9)
Ts10 (64.2)
Ts10 (47.9)
AH1 (-12.8)
Path 1
Path 1
Path 2
Path 2

Figure 7

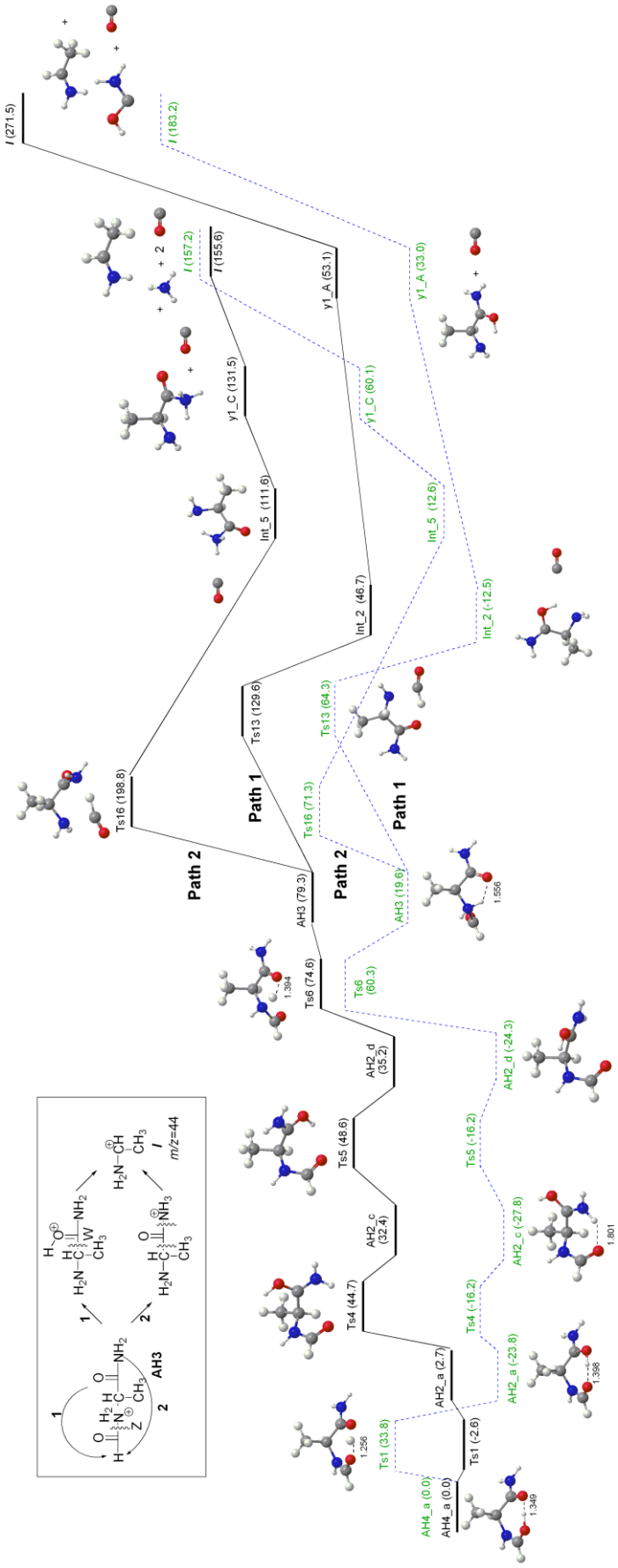
I (271.5)
I' (183.2)
I (157.2)
I (155.6)
y1_A (53.1)
y1_A (33.0)
y1_C (131.5)
y1_C (60.1)
Int_5 (111.6)
Int_5 (12.6)
Int_2 (46.7)
Int_2 (-12.5)
Ts16 (198.8)
Ts13 (129.6)
Ts13 (64.3)
Ts16 (71.3)
Path 2
Path 1
Path 1
Path 2
AH3 (79.3)
AH3 (19.6)
Ts6 (74.6)
Ts6 (60.3)
AH2_d (35.2)
AH2_d (-24.3)
Ts5 (48.6)
Ts5 (-16.2)
AH2_c (32.4)
AH2_c (-27.8)
Ts4 (44.7)
Ts4 (-16.2)
AH2_a (2.7)
AH2_a (-23.8)
Ts1 (33.8)
Ts1 (-2.6)
AH4_a (0.0)
AH4_a (0.0)
1.394
1.556
1.256
1.398
1.349
1.801
AH3
m/z=44

Figure 8

Precursor ion	Product ions			
	(b_1); -NH_3	(y_1); -CO	(a_1); - [H_3,N,C,O]	(*I*); -[H_3,C_2,O_2,N]
[(HCO-Ala-NH_2)H]$^+$ (*m/z* 117)	*m/z* 100	*m/z* 89	*m/z* 72	*m/z* 44
[(DCO-Ala-NH_2)H]$^+$ (*m/z* 118)	*m/z* 101	*m/z* 90	*m/z* 73	*m/z* 44/45
[(H^{13}CO-Ala-NH_2)H]$^+$ (*m/z* 118)	*m/z* 101	*m/z* 89	*m/z* 73	*m/z* 44

Table 1

Product ion	Precursor ion						
	Experimental MS/MS	AH4_a (0.0)	AH4_b (23.7)	AH2_a (2.7)	AH2_c (32.4)	AH1 (68.9)	AH3 (79.3)
b_1 (*m/z* 100)	X	X	X			X	
y_1 (*m/z* 89)	X	X	X				X
a_1* (*m/z* 74)			X		X		
a_1 (*m/z* 72)	X	X	X	X	X	X	X
X_0 (*m/z* 46)		X	X	X	X	X	X
I (*m/z* 44)	X	X	X	X	X	X	X
B_0 (*m/z* 29)				X	X	X	X

Table 2